Engineered Science
DOI: https://dx.doi.org/10.30919/es1801

Hanning-Windowed Compressive Sensing with Interpolation for Power Harmonic Measurement

Chengbin Liang,[1] Yuanda Liu,[1] Guoping Zhang[2,*] and Jianmin Li[3]

Abstract

To mitigate measurement errors caused by spectral leakage and the fence effect in power harmonic detection, while addressing the issues of excessive data volume and slow algorithm reconstruction in traditional methods, this paper proposes a Hanning-windowed compressed sensing and interpolation approach for power harmonic detection. First, the Hanning window is integrated into the compressed sampling process of compressed sensing to achieve windowed compressed sampling of signals. Subsequently, the Binary Search-based Sparse Adaptive Matching Pursuit (BSAMP) algorithm is employed to reconstruct the sparsely sampled vectors. The reconstructed sparse vectors are further refined using a three-spectral-line interpolation technique to obtain the final harmonic parameter estimates. Finally, an experimental platform is constructed to verify the theoretical correctness and practical feasibility of the proposed method. Experimental results demonstrate that, at a compression ratio of 50%, the maximum relative errors for frequency, amplitude, and phase measurements are 0.0074%, -0.33%, and 0.95%, respectively. This confirms the method's capability to accurately detect complex harmonic signals with a reduced number of sampling points. In hardware experiments, the maximum absolute errors for frequency and amplitude measurements are 0.0153Hz and 0.1627V, respectively, further validating the effectiveness and feasibility of the proposed approach.

Keywords: Harmonic measurement; Compressed sensing; Three-spectral-line interpolation; Adaptive matching pursuit algorithm; Hanning window.
Received: 04 July 2025; Revised: 28 September 2025; Accepted: 03 October 2025
Article type: Research article.

1. Introduction

With the rapid increase in grid-connected capacity of renewable energy generation and the widespread application of power electronic devices in power systems, harmonic pollution in power grids has become increasingly severe, leading to progressively prominent power quality issues.[1,2] To ensure the safe and stable operation of power systems and improve power supply quality, accurate detection of harmonic components in power grids has become a critical prerequisite for subsequent harmonic mitigation. Power system harmonic detection primarily utilizes conventional methods such as wavelet transform,[3] Fast Fourier Transform (FFT),[4] and Deep Learning.[5,6] Among these, FFT and its improved algorithms have gained widespread engineering adoption owing to their computational efficiency and implementation simplicity.[7]

However, practical applications reveal that FFT-based harmonic detection suffers from significant accuracy degradation due to spectral leakage and the picket fence effect caused by non-synchronous sampling.[8] To address these limitations, researchers have developed solutions employing windowing techniques to mitigate spectral leakage and interpolation algorithms to overcome the picket fence effect, thereby enhancing frequency resolution and harmonic detection accuracy.[9-11] For instance, K. Wang *et al.*[12] combined a rectangular window with a three-spectral-line interpolation algorithm, effectively suppressing spectral leakage and picket fence effects while demonstrating moderate noise resistance - though its detection accuracy remains unsatisfactory. Y. Deng *et al.*[13] proposed an enhanced method integrating a Nuttall convolution window with an all-phase FFT interpolation algorithm, substantially improving accuracy. Nevertheless, this approach faces practical engineering challenges due to its substantial data volume,

[1]*College of Electrical Engineering, Guizhou University, Guiyang, 550025, China*
[2]*School of Mathematics and Statistics, Guizhou University, Guiyang, 550025, China*
[3]*College of Engineering and Design, Hunan Normal University, Changsha, 410081, China*
[*]*Email*: zhanggp@gzu.edu.cn (Guoping Zhang)

imposing heavy burdens on storage and transmission systems.[14]

According to the Nyquist sampling theorem, FFT-based acquisition of power grid harmonic data necessitates a sampling frequency of at least twice the highest harmonic frequency. However, sustained high-precision sampling inevitably generates exponentially growing data volumes, leading to significant technical challenges including storage limitations, escalating recording costs, and reduced transmission efficiency.[15] Compressed sensing (CS) theory addresses these limitations by fundamentally transforming conventional data acquisition paradigms. This framework enables signal sampling at rates significantly below the Nyquist frequency, simultaneously compressing data during acquisition while maintaining accurate reconstruction from limited measurements.[16-21] T. Yang *et al.*[22] proposes a CS-based harmonic detection method employing the SPG-FF algorithm to achieve low computational complexity and high detection accuracy, however demonstrating limited noise immunity. Y. Niu *et al.*[23] develops an IoT-based real-time monitoring framework utilizing dynamic compressed sensing with sliding-window sampling and homotopy optimization-based recovery to reduce computational complexity and enhance real-time performance, albeit with suboptimal detection accuracy compared to conventional approaches. Consequently, CS's capability for high-fidelity reconstruction from substantially reduced data volumes renders it particularly promising for precise harmonic parameter measurement in power systems.[15,24]

In view of this, this paper proposes a power complex harmonic detection method based on Hanning window compressed sensing and interpolation, which achieves rapid and accurate detection of harmonic parameters while significantly reducing the volume of detection data, thereby addressing the challenges of data storage and transmission. The main contributions of this paper are as follows:

- The Hanning window function is integrated into the compressed sampling process of compressed sensing by constructing a windowed sparse measurement matrix, enabling windowed compressed sampling of harmonic signals. This approach not only effectively alleviates the sampling pressure, data transmission, and storage difficulties in harmonic detection but also significantly suppresses spectral leakage, thereby improving harmonic measurement accuracy.
- Based on the low-dimensional observation vectors and sensing matrix obtained from windowed compressed sampling, the Binary Search-based Sparse Adaptive Matching Pursuit algorithm is employed to accelerate the convergence speed of harmonic signal reconstruction. Simultaneously, a three-spectral-line interpolation technique is utilized to mitigate the picket-fence effect. This achieves rapid harmonic signal detection while effectively enhancing the measurement accuracy of harmonic parameters.
- After extensive simulation experiments validating the superiority of the proposed method in terms of detection accuracy, noise immunity, and robustness, a hardware test platform is constructed. Experimental results demonstrate that the harmonic parameters can be successfully detected within an extremely short time, with a maximum absolute frequency error of 0.0153 and a maximum absolute amplitude error of 0.1627, confirming the practical feasibility of the proposed algorithm.

2. Principles of complex power harmonic detection

2.1 Motivation

The Hanning window function is widely employed in conventional harmonic parameter measurement due to its rapid side lobe attenuation rate and relatively narrow main lobe width. In harmonic detection, it can effectively handle scenarios with numerous frequency components, complex spectral manifestations, and high requirements for frequency resolution, while mitigating measurement errors caused by spectral leakage. On the other hand, CS theory, as an algorithm capable of significantly reducing computational data requirements, integrates the sampling and compression processes into a single step. It enables accurate signal reconstruction with only a minimal amount of data, demonstrating considerable potential in the current field of harmonic detection.

Therefore, to alleviate the computational burden of harmonic detection data, effectively suppress spectral leakage, and improve the measurement accuracy of complex harmonic parameters, this paper integrates a window function into the compressed sampling process of CS technology. Specifically, a windowed sparse measurement matrix is constructed by combining a Gaussian random measurement matrix with the Hanning window function, thereby achieving windowed compressed sampling of harmonic signal data. Subsequently, to address the issue of slow convergence speed in the traditional Sparsity Adaptive Matching Pursuit algorithm, which degrades the real-time performance of signal reconstruction, this paper adopts the Binary Search-based Sparse Adaptive Matching Pursuit algorithm to reconstruct and estimate the compressed-sampled data, thereby accelerating the convergence speed of harmonic signal reconstruction. Finally, to mitigate the fence effect exacerbated by reduced sampling data, a three-spectral-line interpolation technique is employed to correct the reconstructed sparse vector, significantly reducing measurement errors caused by the fence effect and further enhancing the accuracy of harmonic disturbance parameter measurement. The detection process of this method is illustrated in Fig. 1, with the specific steps as follows:

Module 1: The Hanning window function is integrated into the Gaussian random measurement matrix of the CS technique.

This integration constructs a windowed sparse measurement matrix, enabling the windowed compressed

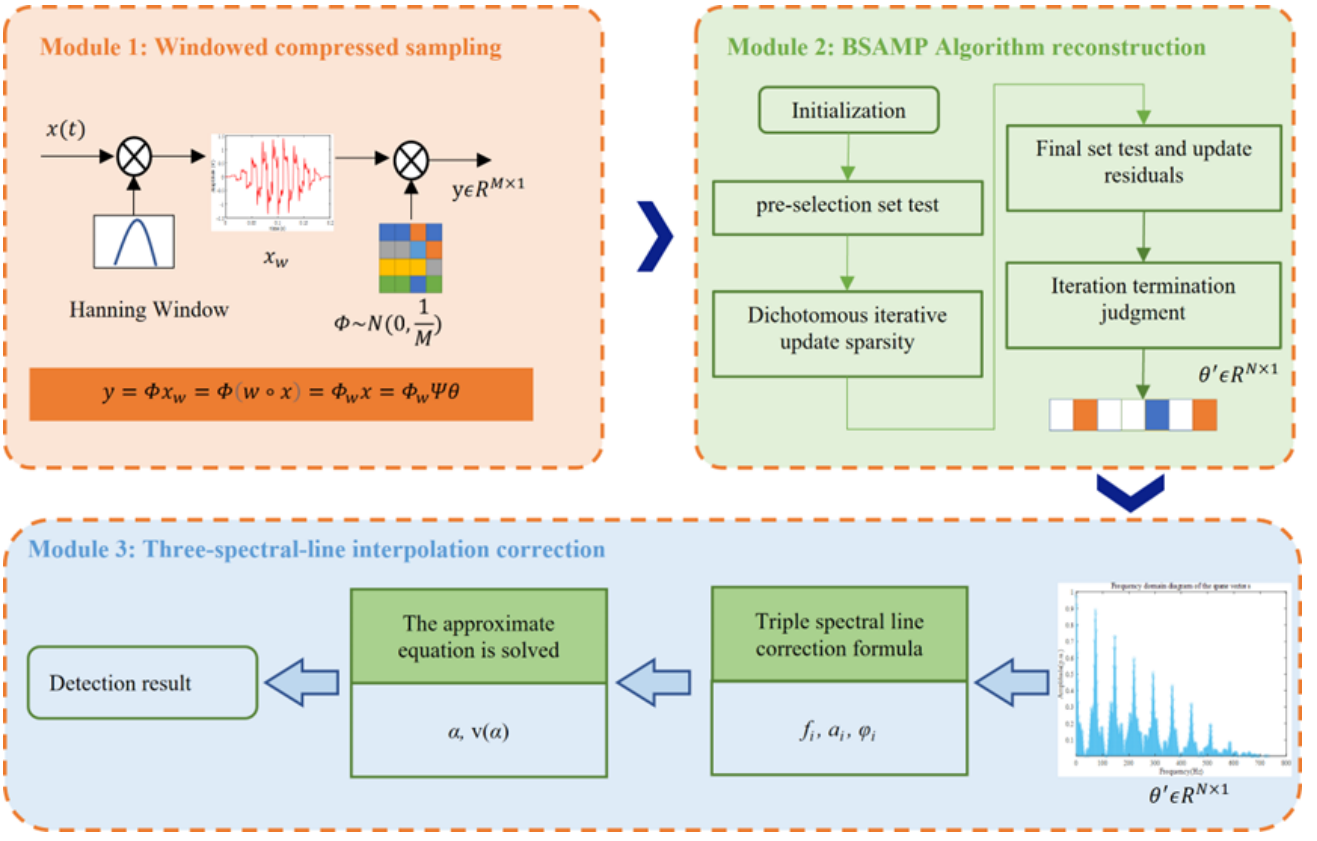

Fig. 1: Harmonic measurement based on windowed compressed sampling and interpolation.

sampling of harmonic disturbance signals.

Module 2: Based on the low-dimensional observation vectors and sensing matrix obtained from windowed compressed sampling, the binary search theory, known for its efficient time complexity and stable search performance, is utilized. The Binary Search-based Sparse Adaptive Matching Pursuit algorithm is employed to reconstruct and estimate the sparse vector obtained from windowed compressed sampling, thereby enhancing the convergence speed of the algorithm.

Module 3: Based on the intermediate variables of the Hanning window function in the three-spectral-line interpolation theory, this module performs interpolation correction on the frequency-domain spectral lines of the reconstructed sparse vector through frequency, amplitude, and phase correction formulas, thereby accurately detecting the characteristic parameters of each harmonic component.

2.2 Windowed compressive sampling based on hanning window and compressive sensing

In this subsection, based on the compressive sensing (CS) method, a windowed sparse measurement matrix is constructed by combining a Gaussian random measurement matrix and the Hanning window function during the compressive sampling process. This approach enables windowed compressive sampling of harmonic signals, which reduces the data processing burden of the harmonic signals while improving the accuracy of harmonic parameter measurements. The steps of the windowed compressive sampling based on the CS method are as follows:

Part 1. This part focuses on the selection of the window function. In general, a window function with a narrower main lobe width exhibits higher frequency resolution and faster sidelobe decay rate, thereby demonstrating stronger capability to suppress interference between frequency components. In power harmonic analysis, harmonic signals typically contain multiple frequency components with complex spectral characteristics, necessitating greater emphasis on the detection of individual frequency points. Consequently, window functions featuring both narrow main lobe width and rapid sidelobe decay rate are more advantageous for harmonic signal detection.

Fig. 2 illustrates the time-frequency characteristics of several commonly used window functions, while Table 1 lists the specific values for the main lobe width, sidelobe peak level, and sidelobe decay rate of these window functions. Combining the information from Table 1 and Fig. 2, it is evident that both the Hanning window and the Hamming window have relatively small main lobe widths, meeting the harmonic detection requirement for high frequency resolution. Additionally, compared to the Hamming window, the Hanning window has a faster sidelobe decay rate, making it more effective at suppressing spectral leakage. Although other window functions have lower sidelobe peak levels or faster sidelobe decay rates, their wider main lobes make them less suitable for the harmonic detection needs outlined in this paper. Therefore, this paper selects the Hanning window to process harmonic signals. The time-domain expression of the Hanning window of length N is given by Eq. (1).

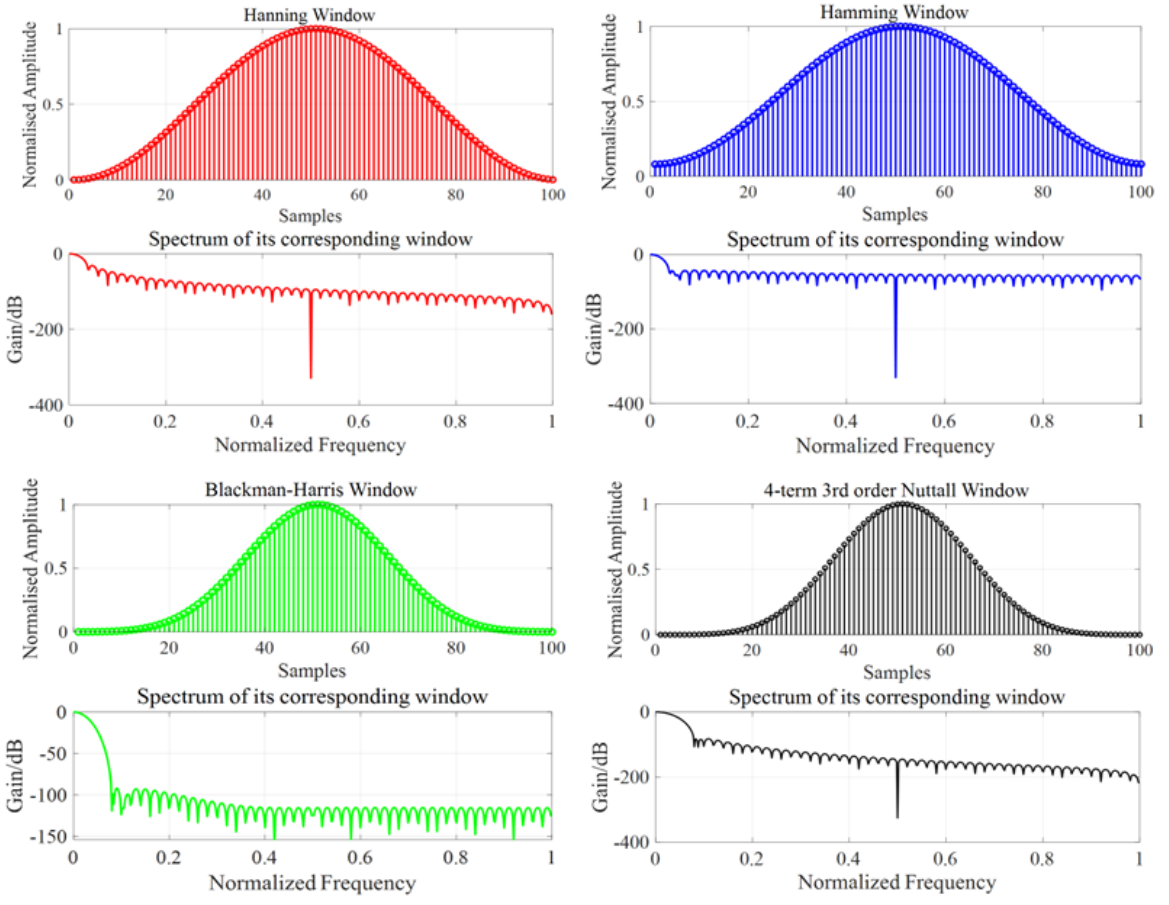

Fig. 2: Comparison of time-frequency plots: Hanning window function versus other window functions.

Table 1: Sidelobe characteristics of commonly used window functions.

Window function	Main lobe width	Sidelobe decay rate	Sidelobe peak level
Hanning	$8\pi/N$	18dB/oct	-32dB
Hamming	$8\pi/N$	6dB/oct	-43dB
Black-harris	$16\pi/N$	6dB/oct	-92dB
4-term 3rd order Nuttall	$16\pi/N$	30dB/oct	-82.6dB

$$w(n) = 0.5 - 0.5\,cos(\frac{2\pi n}{N}) \quad (1)$$

where N is the total number of samples, n=0,1,2,...,N-1.

Part 2. Construction of window sparse measurement matrix for windowed compressed sampling of harmonic signals. The power grid harmonic signal model is given by Eq. (2):

$$x(t) = \sum_{h=1}^{H} A_h cos(2\pi f_h t + \varphi_h) \quad (2)$$

where h represents the h-th harmonic component, A_h is the amplitude, f_h is the frequency, φ_h is the phase, and H is the number of harmonic components. Then, using a Hanning window function $w(n)$ of length N, the discrete sequence $x(n/f_s)$ of the harmonic signal $x(t)$ is windowed and truncated to obtain.

$$x_w(n) = \sum_{h=1}^{H} A_h cos(\frac{2\pi n f_h}{f_s} + \varphi_h)\, w(n) \quad (3)$$

where f_s is the sampling frequency and n=0, 1, 2, ..., N-1.

When the windowed harmonic discrete-time signal $x_w(n) \in R^N$ in Eq. (3) is a sparse signal, a Gaussian random measurement matrix $\Phi \in R^{M \times N} (M \ll N)$ that is uncorrelated with the transformation basis Ψ can be used to perform a linear measurement on the original signal. The resulting observation vector $y \in R^M$ can be expressed as

$$y(m) = \Phi x_w(n) \quad (4)$$

Further, Eq. (4) can be reformulated as

$$y(m) = \Phi\{w(n) \circ x(n)\} = \Phi_w x(n) \quad (5)$$

where $\circ$ denotes the Hadamard product, Φ_w is the $M \times N$

dimensional window sparse measurement matrix. Eq. (5) incorporates windowing information into the Gaussian random measurement matrix, thereby achieving an improvement in the compressive sensing algorithm at the measurement matrix level. This enhanced approach effectively suppresses spectral leakage phenomena while maintaining excellent frequency resolution characteristics.

Part 3. In this part, we construct the sensing matrix A for the CS process. If the harmonic signal from Part 2 is not inherently sparse, it is usually possible to find a specific transformation basis Ψ such that the signal exhibits the desired sparsity when projected onto this basis. This can be represented as

$$x(n) = \Psi s(n) \tag{6}$$

where Ψ denotes the Fourier orthogonal transform matrix that is mutually uncorrelated with the Gaussian random measurement matrix Φ, and θ_n is the sparse representation of the signal $x(n)$

By substituting Eq. (6) into Eq. (5), one can obtain

$$y(m) = \Phi_w x(n) = \Phi_w \Psi \theta(n) = A\theta(n) \tag{7}$$

In this formulation, $A=\Phi_w\Psi\in R^{M\times N}$ is defined as the sensing matrix, where both the window-sparse matrix Φ_w and the composite sensing matrix A must satisfy the Restricted Isometry Property (RIP) conditions.

Part 4. Design of reconstruction algorithm for sparse vector estimation. When M, N, and the sparsity level K satisfy the condition $M\geq K\times\log(N)$, the original signal of length N can be reconstructed using M observations through a signal reconstruction algorithm. Specifically, Eq. (7) can be rewritten in matrix form as

$$\begin{bmatrix} y_1 \\ y_2 \\ \vdots \\ y_M \end{bmatrix} = \begin{bmatrix} A_{11} & \cdots & A_{1N} \\ \vdots & \ddots & \vdots \\ A_{M1} & \cdots & A_{MN} \end{bmatrix} \begin{bmatrix} \theta_1 \\ \theta_2 \\ \vdots \\ \theta_N \end{bmatrix} \tag{8}$$

Further, Eq. (8) can be expressed as a sum of multiple column vectors as given by Eq. (9):

$$\begin{bmatrix} y_1 \\ y_2 \\ \vdots \\ y_M \end{bmatrix} = \theta_1 \begin{bmatrix} A_{11} \\ A_{21} \\ \vdots \\ A_{M1} \end{bmatrix} + \theta_2 \begin{bmatrix} A_{11} \\ A_{21} \\ \vdots \\ A_{M1} \end{bmatrix} + \cdots + \theta_N \begin{bmatrix} A_{1N} \\ A_{2N} \\ \vdots \\ A_{MN} \end{bmatrix} = \theta_1\gamma_1 + \theta_2\gamma_2 + \cdots + \theta_N\gamma_N \tag{9}$$

where $\gamma_i\in R^M$, i=0, 1, 2, ..., N is the corresponding column vector of the perception matrix A. Since the sparse vector θ_n is K-sparse, meaning that θ_i, i=0, 1, 2, ..., N contains K non-zero elements, design of reconstruction algorithm is used to identify these K non-zero values.

Based on the aforementioned conditions, the present paper employs a binary search-based improved sparse adaptive matching pursuit (SAMP) algorithm in the following sections to accurately reconstruct the sparse vector θ_n using the observation values $y(m)$, the sensing matrix A, and the step size θ_n as input parameters.

2.3 Binary search-based improved SAMP for fast reconstruction algorithm

The traditional SAMP algorithm differs from other OMP-based algorithms in that it does not require prior knowledge of the signal sparsity K, and can progressively approach the sparse vector by adaptively adjusting the step size. However, it suffers from issues such as linear approximation and the lack of a backtracking mechanism in the iterative model, which degrades the real-time performance of signal reconstruction. To address this, this paper utilizes the binary search theory, known for its efficient time complexity and stable search performance. We propose a Binary Search-based Improved Fast SAMP Reconstruction Algorithm (BSAMP) to reconstruct the sparse vector θ_n. By reducing the number of searches for the optimal sparsity, the BSAMP algorithm accelerates the convergence speed of the reconstruction process.

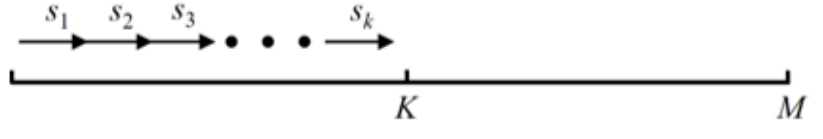

(a) Linear approximation sparsity K.

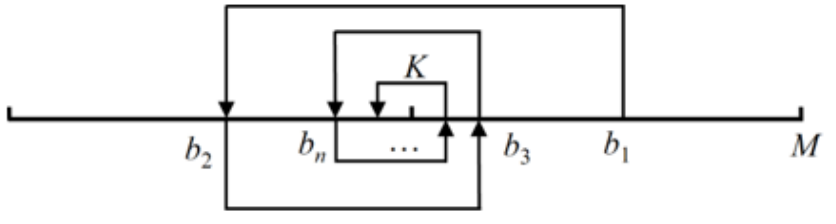

(b) Bisection method approximation sparsity K.

Fig. 3: The diagram of optimal sparsity approximation.

Table 2: The process of the BSAMP reconstruction algorithm.

BSAMP Algorithm Process
Input: Sensing matrix A, observation vector y, threshold ε, iteration interval $[L,R]$
Initialization: residual $r_0=y$, support set $F_0=\emptyset$, index set $S_0=\emptyset$, and candidate set $C_0=\emptyset$
while($L<R$)
for($s=mid$; $s\leq mid+1$; s++)
$mid=(L+R)/2$
$S_k=\max(\lvert\phi_{r\,k-1}\rvert, mid)$ {initial test}
$C_k=F_{k-1}\cup S_k$; {Merge the index set and the support set}
$F=\max(\lvert\phi^{+}_{ck}, L)$ {Final test}
$r=y-\phi_F\phi^{+}_F y$ {Update the residual}
if(r<δ)
$\theta=\phi^{+}_F y$ {Meet the iteration accuracy of the SAMP algorithm}
Break; {End the iteration}
else
$F_k=F$, $r_k=r$; {Update the final set}
k++;
if($\Delta_k<\varepsilon$) {If less than or equal to the threshold, update the right boundary}
$R=mid$;
else {If greater than the threshold, update the left boundary}
$L=mid+1$;
Output: Sparse vector θ

In Fig. 3(a) and (b) illustrate the approximation of sparsity K during the reconstruction process using linear approximation and the bisection method in the traditional SAMP and BSAMP algorithms, respectively. The traditional SAMP algorithm, when the optimal sparsity K is large, requires multiple iterations, leading to significant reconstruction time consumption, with a time complexity of $O(M)$, and may also result in incorrect sparsity estimation. In contrast, the BSAMP algorithm uses the bisection method to approximate the optimal sparsity with a time complexity of $O(\log_2 M)$. As shown in Fig. 3(b), the BSAMP algorithm starts with the midpoint b_1 of the segment as the preset starting point and, at each iteration, selects the midpoint of the interval to divide the valid interval until the midpoint of the interval converges to the target point K. This approach reduces the number of iterations and accelerates the algorithm's convergence speed. The iterative steps of the BSAMP algorithm are shown in Table 2.

2.4 Measurement of harmonic parameters based on three-spectral-line interpolation

The FFT of the windowed signal $x_w(n)$ from Eq. (3) yields

$$X_W(f)=\sum_{h=1}^{H}\frac{A_h}{2j}\{e^{j\varphi_h}W[\frac{2\pi}{f_s}(f-f_h)]-e^{j\varphi_h}W[\frac{2\pi}{f_s}(f+f_h)]\} \quad (10)$$

where $W(f)$ is the frequency spectral of window $w(n)$.

By discretely sampling Eq. (10) and neglecting the side-lobe effects at the frequency peaks corresponding to negative frequencies, the FFT expression of the windowed signal can be given by Eq. (11):

$$X(k\Delta f)=\sum_{h=1}^{H}\frac{A_h}{2j}e^{j\varphi_h}W[\frac{2\pi(k\Delta f-f_h)}{f_s}] \quad (11)$$

where $\Delta f=f_s/N$.

In the signal non-synchronous sampling or non-integer cycle truncation, when $k=f_0/\Delta f=Nf_h/f_s$ is a non-integer, the signal frequency may not align with the discrete frequency spectrum. After the BSAMP algorithm estimates the sparse vector θ representing the windowed harmonic frequency spectrum information, frequency deviations caused by the picket-fence effect make it challenging to accurately measure the harmonic components. To address this issue, spectral interpolation techniques are generally employed to correct the spectral lines of the sparse vector. These techniques include two-line interpolation, three-line interpolation, and four-line interpolation, among others. While two-line interpolation performs poorly for harmonic signals with multiple frequency components, four-line interpolation offers higher detection accuracy but suffers from higher complexity and slower correction speed. In contrast, three-line interpolation strikes a balance between detection accuracy and correction speed, making it suitable for interpolating and correcting the sparse vector to accurately estimate the characteristic parameters of each harmonic component.

The three-spectral-line interpolation principle, as illustrated in Fig. 4, utilizes the amplitude values of the main spectral line k_1 and its adjacent spectral lines k_2 and k_3 to perform interpolation, thereby providing a more accurate estimation of the actual frequency position. The correction

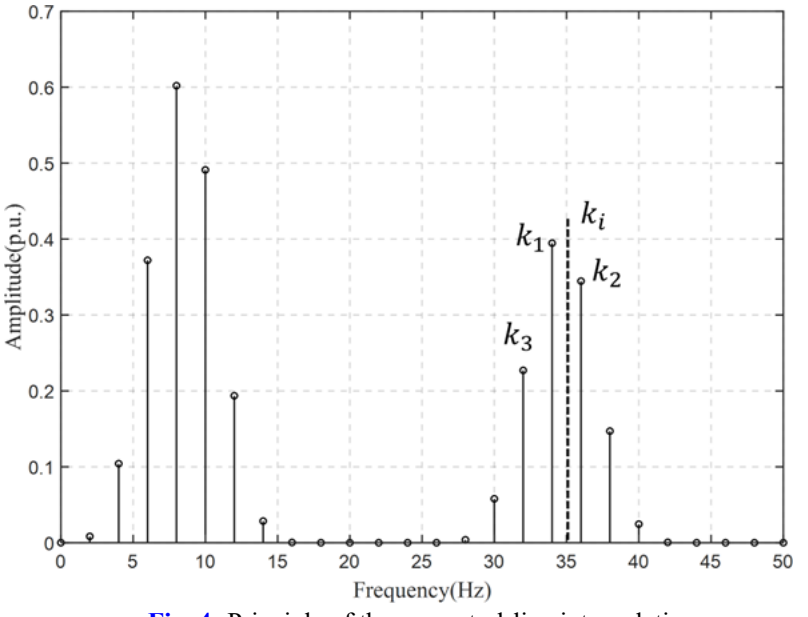

Fig. 4: Principle of three-spectral-line interpolation.

formulas for the frequency, amplitude, and phase of the harmonic components are given by Eq. (12):

$$\begin{cases} a_i = \dfrac{(y_1 + 2y_2 + y_3)v(\alpha)}{N} \\ f_i = \dfrac{(\alpha + k_i - 1)f_s}{N} \\ \varphi_i = arg(\hat{s}(k_i)) - \alpha\pi \end{cases} \tag{12}$$

where f_i, a_i, φ_i are the requested frequency, amplitude, and phase, respectively, f_s is the sampling frequency, y_1, y_2, and y_3 are the amplitudes of k_1, k_2, and k_3, α is the offset, with a range of [-0.5,0.5].

Through polynomial fitting, the approximate expressions for the intermediate variables α and $v(\alpha)$ of the Hanning window function are given by Eq. (13):

$$\begin{cases} \alpha\&=0.66666287b\text{-}0.07398320b^3+ \\ 0.01587358b^5\text{-}0.00311639b^7 \\ v(\alpha)=1.33333327+ \\ 0.52658791b^2+0.11699742b^4+ \\ 0.02103885b^6 \end{cases} \tag{13}$$

where $\beta=(y_3\text{-}y_2)/y_1$.

The use of three-spectral-line interpolation technology can effectively mitigate the impact of the picket-fence effect, thereby improving the precision of frequency, amplitude, and phase measurements for harmonic disturbances.

3. Simulation verification and result analysis

3.1 Analysis of non-integer order complex harmonic detection

In the actual operation of the power grid, interference from non-integer order harmonics (inter-harmonics) may occur. To verify the effectiveness of the method proposed in this paper, a signal containing 5 harmonic components and 2 inter-harmonic components is generated using MATLAB for testing. The harmonic disturbance signal model, as shown in Eq. 2, is considered for simulation analysis. The sampling frequency is set to 5120Hz, with 1024 sampling points and a compression ratio(CR) of 50%. The frequency, amplitude, and phase parameters of the harmonic test signal are listed in Table 3.

The improved ICA-OMP algorithm, proposed by Li Yaxin *et al.*,[25] is a harmonic detection method that introduces an enhanced Imperialist Competitive Algorithm (ICA) into the OMP algorithm. This allows for the search of the optimal matching atoms in a continuous parameter space, significantly reducing the computational complexity of the algorithm. Scholars both domestically and internationally have addressed the issue of spectral leakage and the fence effect in harmonic detection using the FFT algorithm, proposing a series of windowed interpolation FFT algorithms. These algorithms can improve the detection accuracy of harmonic frequencies, amplitudes, and phases, while reducing the errors caused by the fence effect. Therefore, in this paper, the improved ICA-OMP algorithm, Hanning windowed interpolation FFT (WI-FFT) algorithm, and the proposed windowed compressive sensing and BSAMP (WCS-BSAMP) detection algorithm are utilized to detect the harmonic disturbance signal from Table 3, with the resulting relative detection errors of various harmonic and inter-harmonic components presented in Table 4.

The detection results indicate that the proposed WCS-BSAMP detection algorithm significantly outperforms the improved ICA-OMP algorithm and WI-FFT in terms of detection accuracy for all component parameters. The maximum relative errors for frequency, amplitude, and phase are 0.0074%, -0.33%, and 0.95%, respectively, achieving precise detection of harmonic characteristic parameters.

In terms of computational complexity, the proposed WCS-BSAMP algorithm requires only 0.16578 seconds, which is significantly faster than the WI-FFT algorithm (0.37658

Table 3: Parameters of other types of harmonic test signals.

Harmonic types	Frequency/Hz	Amplitude/V	Phase/(°)
Fundamental wave	50	1	60
3th harmonic	150	0.3	120
interharmonic 1	167	0.15	130
5th harmonic	250	0.25	110
interharmonic 1	337	0.12	140
7th harmonic	350	0.2	120
9th harmonic	450	0.15	110

Table 4: Relative Error of Different Harmonic Detection Methods (%).

harmonic types	WI-FFT			Improved ICA-OMP			WCS-BSAMP		
	Frequency	Amplitude	Phase	Frequency	Amplitude	Phase	Frequency	Amplitude	Phase
fundamental wave	2.48×10^{-4}	-0.024	-0.024	0.0052	0.0490	/	-9.15×10^{-4}	0.0059	0.0052
3th harmonic	0.0074	-0.045	-0.54	0.0066	0.2222	/	0.0074	-0.0067	-0.55
interharmonic 1	0.0081	0.40	-0.36	0.0051	0.6427	/	-5.9×10^{-4}	-0.22	-6.3×10^{-4}
5th harmonic	6.08×10^{-4}	0.17	-0.037	0.0089	0.2340	/	-9.11×10^{-4}	-0.04	0.049
interharmonic 2	-0.0036	0.32	0.26	0.0018	0.8237	/	-0.0015	0.13	0.0029
7th harmonic	-0.01	0.36	1.70	0.0092	0.4750	/	-0.0080	-0.33	0.95
9th harmonic	-0.0014	-0.42	0.3	0.0058	0.8237	/	3.63×10^{-5}	0.11	0.0068

Table 5: Comparison of the absolute errors of harmonic detection parameters under different window functions.

	Set value	50	150	167	250	337	350	450
Frequency/Hz	4-termminimum sidelobeNuttall	0.018	-0.00213	-0.0548	0.0162	0.0459	-0.1648	-0.0059
	Hamming	-0.0140	-0.0443	1.6400	0.0303	2.7051	-0.0710	-0.0228
	Black-harris	0.0028	-0.0383	-0.4448	0.0442	0.2999	-0.2698	-0.0292
	Hanning	0.0012	3.18×10^{-4}	0.0054	-0.0029	0.007	-0.0256	7.94×10^{-4}
Amplitude/V	Set value	1	0.3	0.15	0.25	0.12	0.2	0.15
	4-termminimum sidelobeNuttall	-0.087	0.0043	-0.0567	-0.0247	0.0075	-0.0856	0.0058
	Hamming	0.0017	0.0016	0.0085	2.89×10^{-4}	0.0093	6.42×10^{-5}	7.86×10^{-4}
	Black-harris	0.0347	0.0079	0.0037	0.0077	2.01×10^{-4}	0.0050	0.0055
	Hanning	-3.14×10^{-5}	4.85×10^{-4}	0.0011	1.52×10^{-4}	1.30×10^{-4}	3.57×10^{-4}	0.0011
Phase/°	Set value	60	120	130	110	140	120	110
	4-termminimum sidelobeNuttall	0.0828	-0.0583	0.0268	0.0472	-0.0685	-0.0618	-0.0192
	Hamming	0.0080	0.0296	-1.0362	-0.0148	-1.7073	0.0391	0.0229
	Black-harris	-2.13×10^{-4}	0.0348	0.3122	-0.0353	-0.1687	0.1347	0.0284
	Hanning	-6.32×10^{-4}	-0.0045	-0.0056	0.0024	-0.0076	0.0284	-0.0011

seconds), demonstrating superior computational efficiency. Furthermore, even at a 50% compression ratio, the WCS-BSAMP algorithm achieves high-precision detection of harmonic disturbance signals. While maintaining high detection accuracy, it substantially reduces the data volume by half, thereby offering distinct advantages in data transmission and storage.

3.2 Analysis of the impact of window functions

To highlight the effectiveness and feasibility of the Hanning window, this paper adds different window functions under the same theoretical framework to detect and analyze the harmonic signals in Table 3. The sampling frequency is set to 5120Hz, with a sampling point number of N=1024 and a compression ratio of CR=50%. The detection results of the harmonic characteristic parameters are presented in Table 5.

The simulation analysis results show that the harmonic detection accuracy with the Hanning window is significantly

better than that with the Hamming window, Black-Harris window and 4-term minimum sidelobe Nuttall. The maximum absolute errors for frequency, amplitude, and phase are -0.0256, 0.0011, and 0.0284, respectively, fully meeting the detection accuracy requirements of the harmonic monitoring system. Therefore, the Hanning window is more suitable for handling complex harmonic situations in this algorithm, enabling precise detection of harmonic signal parameters.

3.3 Analysis of the impact of fundamental frequency fluctuations and white noise on integer-order harmonics

In practical applications, grid signals are subject to fluctuations in the fundamental frequency or white noise, which causes changes in the spectral leakage between the harmonic components of the signal, thereby affecting the accuracy of harmonic parameter estimation. Therefore, to further test the harmonic detection performance of the algorithm proposed in this paper under the influence of both fundamental frequency fluctuations and white noise, a harmonic test signal as shown in Table 6 was generated using MATLAB simulation. The fundamental frequency of the harmonic test signal fluctuates between 49.6Hz and 50.5Hz with a step size of 0.1Hz, and 30dB of random Gaussian white noise is added. The compression ratio CR is set to 50%. The relative errors of the various parameters are then calculated, and the detection results are shown in Fig. 5.

The results show that the relative error range of the frequency parameters for each harmonic component is between 1.56×10^{-5} and 0.091%, with most errors being less than 0.04%. The relative error range for amplitude is between

Table 6: Verification of harmonic test signal parameters under fundamental frequency fluctuation.

Harmonic number	1	3	5	7	9	11	13
Amplitude/(V)	220	66	55	44	33	22	11
Phase/(°)	60	120	130	110	140	120	110

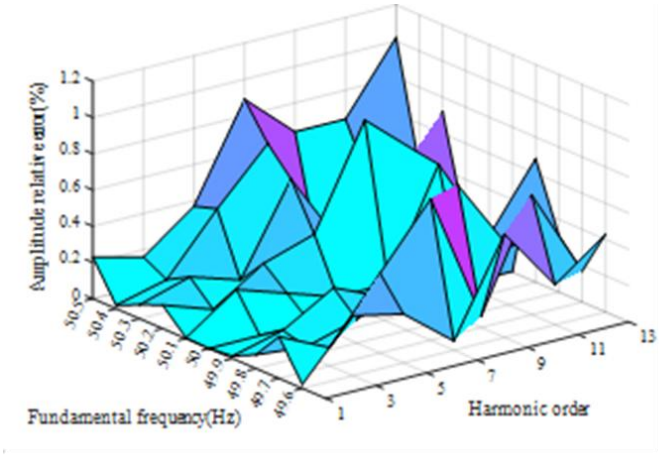

(a) Amplitude

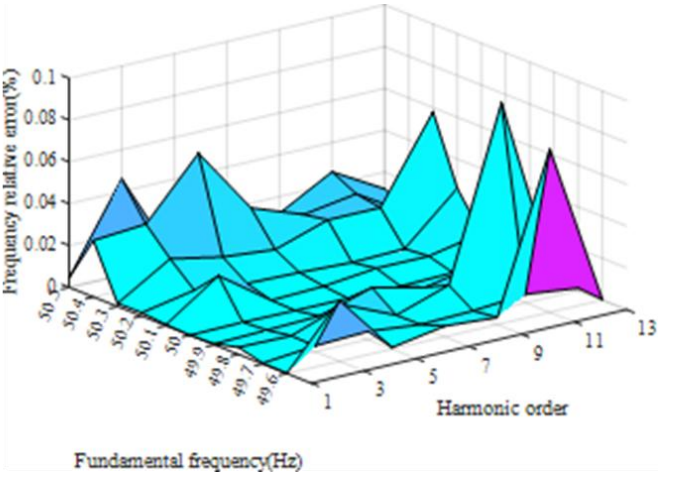

(b) Frequency

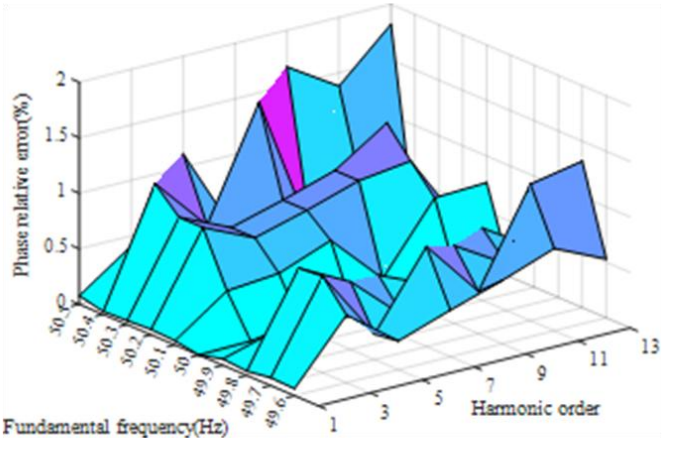

(c) Phase

Fig. 5: Relative error of harmonic characteristic parameters under the fluctuation of fundamental frequency.

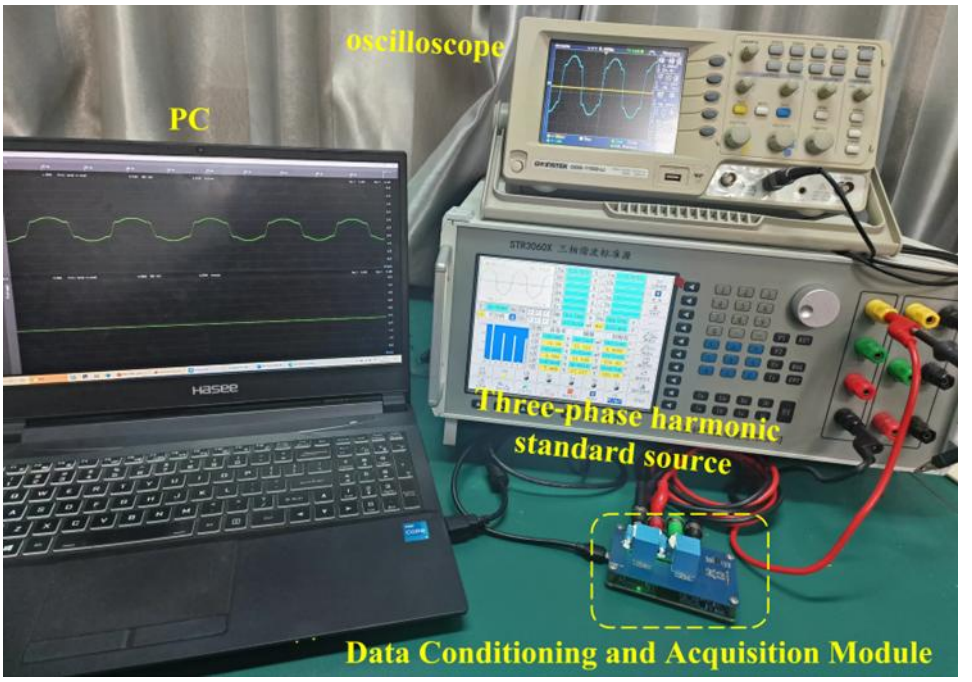

Fig. 6: Harmonic detection hardware experiment platform.

4.91×10^{-4} and 1.02%, and the relative error range for phase is between 0.0014% and 1.82%. The detection results for all parameters show minimal fluctuation, demonstrating good robustness. Therefore, the WCS-BSAMP detection algorithm proposed in this paper can well detect the complex harmonics under the simultaneous influence of frequency fluctuation and white noise.

4. Experiment setup verification and BSAMP performance analysis

To further verify the practical feasibility of the detection algorithm proposed in this paper, a hardware simulation platform is constructed to conduct actual measurements and analysis of the harmonic disturbance signal parameters (considering only frequency and amplitude) shown in Table 6. The hardware detection platform is shown in Fig. 6.

The detection process of the hardware platform is as follows: First, the STR3060X three-phase harmonic standard source generates the harmonic test signal, while an oscilloscope is used to monitor the waveform of the harmonic test signal in real-time. Next, the signal conditioning module converts the test signal into an analog signal that fits the voltage input range of the data acquisition module (ADALM1000 data acquisition card). After the data acquisition card samples the signal, communication with the host PC is established via the USB interface. Finally, the MATLAB simulation software on the PC applies the algorithm proposed in this paper to perform measurement and analysis of the collected harmonic signal data.

4.1 Hardware simulation results and BSAMP reconstruction performance analysis

In the actual measurement, the sampling frequency of the ADALM1000 data acquisition card was set to 100kHz with a sampling time of 100ms. The execution time of the algorithms was measured using MATLAB's built-in tic/toc functions. The hardware platform consisted of an Intel Core i5-11400H processor (with a maximum turbo frequency of 2.7GHz) and 16GB of DDR4 memory. The harmonic test signal generated by the three-phase harmonic standard source, as shown in Table 6, was conditioned and acquired. The peak and trough values of the obtained signal were 3.0099V and 1.7317V, respectively. Calculations show that after conditioning, the peak-to-peak value of the signal was reduced from $440\sqrt{2}$ to 1.2782V, a reduction factor of 486.8205 times. Meanwhile, its voltage was increased by 2.3708V. Therefore, the harmonic test signal sampled needs to be reduced by 2.3708V and its voltage amplitude amplified by 486.8205 times to restore the actual harmonic test signal. Finally, the harmonic detection algorithm proposed in this paper was applied for testing and verification. The waveform of the harmonic test signal after sampling and adjustment is shown in Fig. 7.

To verify the advantage of the BSAMP algorithm in terms of fast reconstruction convergence, this paper applies the BSAMP algorithm, Sparse Adaptive Matching Pursuit (SAMP) algorithm, and Orthogonal Matching Pursuit (OMP) algorithm for Hanning windowed reconstruction estimation of the test signal shown in Fig. 7, with a compression ratio set to 12.5%. The reconstruction times for SAMP, OMP, and BSAMP are 92.9237s, 0.7670s, and 0.2177s, respectively, demonstrating the superior convergence performance of the BSAMP algorithm.

Fig. 8 shows a comparison between the signal reconstructed using the BSAMP algorithm after windowing and the original windowed signal. As can be seen from the figure, with a compression ratio of only 12.5%, the

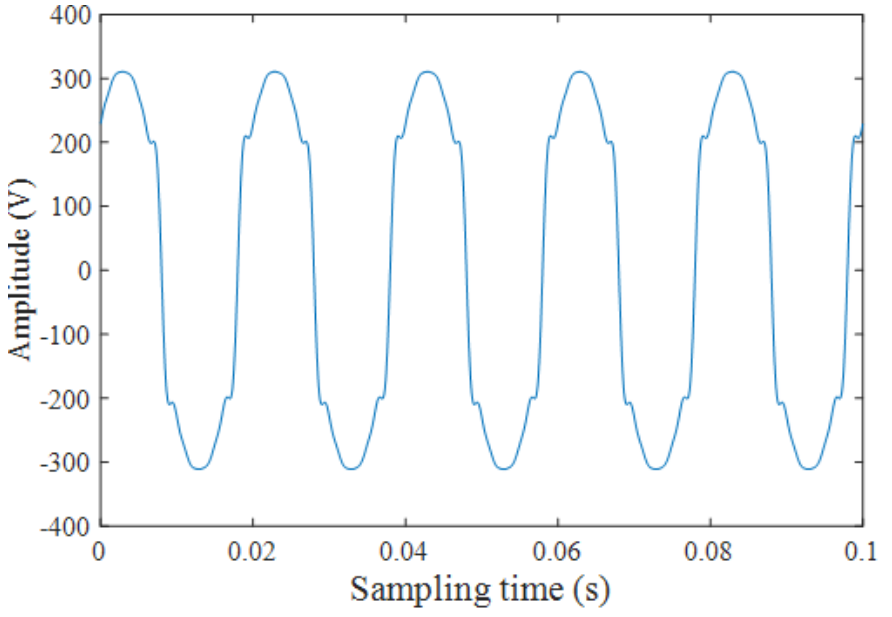

Fig. 7: Adjusted harmonic test signal after sampling.

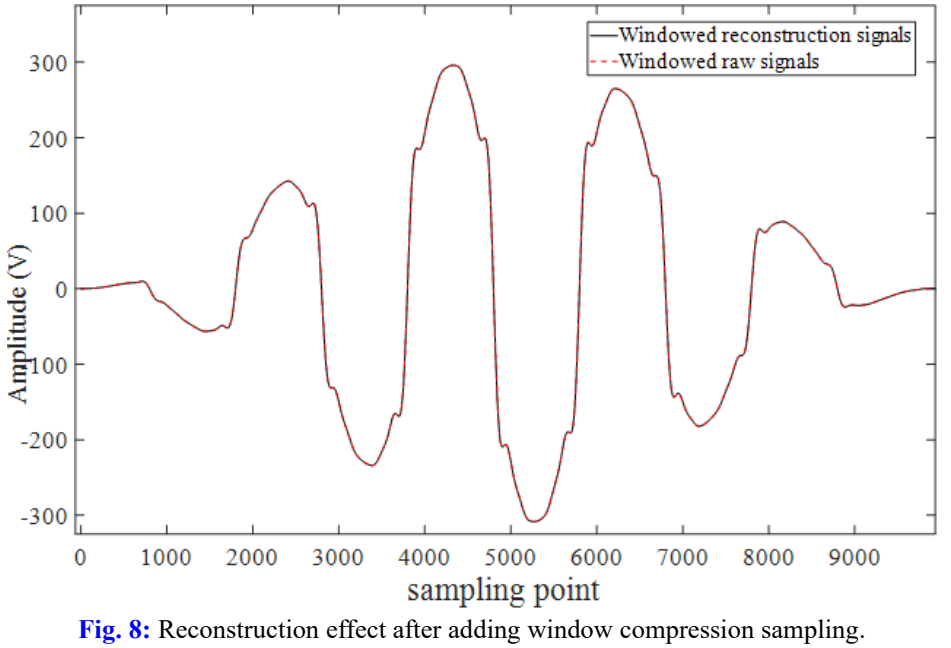

Fig. 8: Reconstruction effect after adding window compression sampling.

Table 7: Harmonic parameter detection results of hardware platform.

Frequency (Hz)				Amplitude (V)			
Set value	SAMP	OMP	BSAMP	Set value	SAMP	OMP	BSAMP
50	50.0011	50.0007	50.0011	220	219.8709	219.8679	219.8770
150	150.0024	150.0032	150.0016	33	33.1562	33.1723	33.1627
250	250.0058	250.0054	250.0023	20	22.0892	22.0994	22.0858
350	350.0044	350.0056	350.0117	17.6	17.6820	17.6869	17.6970
450	450.0083	450.0043	450.0053	11	11.0480	11.0449	11.0366
550	550.0214	550.0091	550.0307	6.6	6.6192	6.6286	6.6126
650	650.0009	650.0146	650.0153	2.2	2.2098	2.2052	2.1946

reconstruction accuracy is relatively high, significantly reducing the data required for harmonic detection. This preliminarily verifies the practical feasibility of the window function and CS technology used in this paper for harmonic detection. The harmonic characteristic parameter detection results, as shown in Table 7, indicate that the maximum absolute error for the frequency and amplitude reconstructed using the BSAMP algorithm is 0.0153Hz and 0.1627V, respectively. The measurement accuracy meets the requirements for harmonic parameter detection. This further validates the advantage of the BSAMP algorithm in achieving fast reconstruction convergence while maintaining high detection accuracy, and also confirms the practical application value of the harmonic detection algorithm proposed in this paper in the field of harmonic detection.

5. Conclusion

This paper investigates a harmonic detection method based on Hanning window compressed sensing and interpolation. At the sampling end, a windowed sparse measurement matrix is constructed to compressively sample harmonic signals, effectively mitigating the impact of spectral leakage and addressing issues related to the large volume of harmonic detection data, such as problems in storage and transmission. At the reconstruction end, the paper employs the BSAMP algorithm, which converges quickly and has good real-time performance, to reconstruct and estimate the sparse vector. Additionally, a three-line spectral interpolation technique is used to correct the spectral lines of the sparse vector in the frequency domain, avoiding measurement errors caused by the fence effect. Finally, a harmonic detection experimental platform based on a three-phase harmonic standard source and signal conditioning and acquisition module is established. Simulation and hardware experimental results indicate that, compared to commonly used harmonic detection methods, the proposed method offers advantages in terms of real-time performance, detection accuracy, and reduced data volume, demonstrating practical application value in the field of harmonic detection.

Acknowledgments

This work was jointly supported by the Guizhou Provincial Key Technology R&D Program under Grant 2024[General]136, the Guizhou Provincial Basic Research Program (Natural Science) under Grant MS [2025]600, and the Natural Science Special Research Foundation of Guizhou University under Grant 202313.

Conflict of Interest

To ensure the objectivity and impartiality of academic research, the authors of this article hereby declare that there are no commercial, financial, or personal relationships that could be construed as potential conflicts of interest during the research, data analysis, writing, and publication of this article. This includes, but is not limited to, improper financial support from any organization, equity relationships, advisory positions, or any commitments that may inappropriately influence the interpretation of the research findings.

Supporting Information

Not applicable.

CRediT Statement

Chengbin Liang: Writing – Original draft, Software, Hardware, Methodology, Conceptualization. **Yuanda Liu:** Validation, Methodology, Data curation. **Guoping Zhang:** Writing – Review & editing, Methodology, Funding acquisition, Conceptualization. **Jianmin Li:** Validation, Investigation, Conceptualization.

References

[1] Z. Liu, Distributed power storage and converter system health monitoring internet of things under blockchain, *Information Sciences*, 2023, **645**, 119329, doi: 10.1016/j.ins.2023.119329.

[2] Y. Wang, Y. Hao, K. Zhao, Y. Yao, Stochastic configuration networks for short-term power load forecasting, *Information Sciences*, 2025, **689**, 121489, doi: 10.1016/j.ins.2024.121489.

[3] P. Khatua, K. C. Ray, VLSI architecture of DCT-based harmonic wavelet transform for time - frequency analysis, *IEEE Transactions on Instrumentation and Measurement*, 2023, **72**, 6502108, doi: 10.1109/TIM.2023.3259023.

[4] J. Zhang, J. Song, C. Li, X. Xu, H. Wen, Novel frequency estimator for distorted power system signals using two-point iterative windowed DFT, *IEEE Transactions on Industrial Electronics*, 2024, **71**, 13372-13383, doi: 10.1109/TIE.2023.3347846.

[5] S. Janpong, K. Areerak, K. Areerak, Harmonic detection for shunt active power filter using ADALINE neural network, *Energies*, 2021, **14**, doi:10.3390/en14144351.

[6] Q. Yue, R. Hu, X. Zhang, A power system harmonic problem based on the BP neural network learning algorithm, *Computational Intelligence and Neuroscience*, 2022, **2022**, 7247881, doi: 10.1155/2022/7247881.

[7] C. Liang, Z. Teng, J. Li, W. Yao, L. Wang, Q. He, S. Hu, Improved S-transform for time-frequency analysis for power quality disturbances, *IEEE Transactions on Power Delivery*, 2021, **37**, 2942-2952, doi: 10.1109/TPWRD.2021.3119918.

[8] Z. Jin, H. Zhang, V. Terzija, An embedded estimator for online harmonic monitoring in power-electronic grids, *IEEE Transactions on Smart Grid*, 2022, **13**, 4677-4689, doi: 10.1109/TSG.2022.3186341.

[9] C. Liang, Z. Teng, J. Li, W. Yao, S. Hu, Y. Yang, Q. He, A Kaiser window-based S-transform for time-frequency analysis of power quality signals, *IEEE Transactions on Industrial Informatics*, 2021, **18**, 965-975, doi: 10.1109/TII.2021.3083240.

[10] D. Belega, D. Petri, Fast procedures for accurate parameter estimation of sine-waves affected by noise and harmonic distortion, *Digital Signal Processing*, 2021, **114**, 103035, doi: 10.1016/j.dsp.2021.103035.

[11] Y. Li, Y. Gao, Y. Feng, Y. Cao, Y. Zhu, Improved analytic energy operator and novel three-spectral line interpolation DFT method for parameter estimation of voltage flicker, *IEEE Transactions on Industrial Informatics*, 2023, **20**, 327-336, doi: 10.1109/TII.2023.3261885.

[12] K. Wang, H. Wen, G. Li, Accurate frequency estimation by using three-point interpolated discrete Fourier transform based on rectangular window, *IEEE Transactions on Industrial Informatics*, 2021, **17**, 73-81, doi: 10.1109/TII.2020.2981542.

[13] Y. Deng, G. Zhao, K. Zhu, T. Zhou, Z. Xu, NCAFI: Nuttall convolution window all-phase FFT interpolation-based harmonic detection algorithm for infrared imaging detection, *Infrared Physics & Technology*, 2022, **125**, 104310, doi: 10.1016/j.infrared.2022.104310.

[14] J. Liu, W. Zhao, S. Li, Compressive sensing empirical wavelet transform for frequency-banded power measurement considering interharmonics, *IEEE Transactions on Instrumentation and Measurement*, 2025, **74**, 1503012, doi: 10.1109/TIM.2025.3551123.

[15] R. Arie, A. Brand, S. Engelberg, Compressive sensing and sub-nyquist sampling, *IEEE Instrumentation & Measurement Magazine*, 2020, **23**, 94-101, doi: 10.1109/MIM.2020.9062696.

[16] P. Daponte, L. De Vito, F. Picariello, S. Rapuano, E. Remondini, C. Schettini, I. Tudosa, A compressed-sensing system for radio spectrum monitoring and localization of noncooperative sources, *IEEE Transactions on Instrumentation and Measurement*, 2024, **73**, 3001311, doi: 10.1109/TIM.2024.3395326.

[17] J. Chen, S. Sun, L.-B. Zhang, B. Yang, W. Wang, Compressed sensing framework for heart sound acquisition in Internet of medical things, *IEEE Transactions on Industrial Informatics*, 2022, **18**, 2000-2009, doi: 10.1109/TII.2021.3088465.

[18] Q. Liu, L. Wu, Y. Jin, Federated bayesian optimization via compressed sensing, *Information Sciences*, 2024, **681**, 121148, doi: 10.1016/j.ins.2024.121148.

[19] C. Wang, L. Song, An image encryption scheme based on chaotic system and compressed sensing for multiple application scenarios, *Information Sciences*, 2023, **642**, 119166, doi: 10.1016/j.ins.2023.119166.

[20] Z. Gao, Y. Guo, J. Zhang, T. Zeng, G. Yang, Hierarchical perception adversarial learning framework for compressed sensing MRI, *IEEE Transactions on Medical Imaging*, 2023, **42**, 1859-1874, doi: 10.1109/TMI.2023.3240862.

[21] W. Fu, T. Lu, S. Li, Context-aware compressed sensing of hyperspectral image, *IEEE Transactions on Geoscience and Remote Sensing*, 2020, **58**, 268-280, doi: 10.1109/TGRS.2019.2936229.

[22] T. Yang, H. Pen, D. Wang, Z. Wang, Harmonic analysis in integrated energy system based on compressed sensing, *Applied Energy*, 2016, **165**, 583–591, doi: 10.1016/j.apenergy.2015.12.058.

[23] Y. Niu, T. Yang, F. Yang, X. Feng, P. Zhang, W. Li, Harmonic analysis in distributed power system based on IOT and dynamic compressed sensing, *Energy Reports*, 2022, **8**, 2363–2375, doi: 10.1016/j.egyr.2022.01.119.

[24] D. Carta, C. Muscas, P. A. Pegoraro, S. Sulis, Identification and estimation of harmonic sources based on compressive sensing, *IEEE Transactions on Instrumentation and Measurement*, 2018, **68**, 95-104, doi: 10.1109/TIM.2018.2838738.

[25] Y. Li, Z. Teng, Q. Tang, Z. Ji, Detection of interharmonics using sparse signal decomposition based on ICA-MP, *IEEE Transactions on Instrumentation and Measurement*, 2021, **70**, 9005509, doi: 10.1109/TIM.2021.3122185.